THE JOURNAL OF PHYSICAL CHEMISTRY C

Article

pubs.acs.org/JPCC

Linear and Nonlinear Optical Properties of Graphene Quantum Dots: A Computational Study

Sharma S. R. K. C. Yamijala,[†] Madhuri Mukhopadhyay,[‡] and Swapan K. Pati*[,‡]

[†]Chemistry and Physics of Materials Unit, Jawaharlal Nehru Centre for Advanced Scientific Research, Bangalore 560064, India

[‡]Theoretical Sciences Unit, Jawaharlal Nehru Centre for Advanced Scientific Research, Bangalore 560064, India

Supporting Information

ABSTRACT: Because of the advantages of tunability via size, shape, doping, and relatively low level of loss and high extent of spatial confinement, graphene quantum dots (GQDs) are emerging as an effective way to control light by molecular engineering. The collective excitation in GQDs shows high energy plasmon frequency along with frequencies in the terahertz (THz) region, making these systems powerful materials for photonic technologies. Here, we report a systematic study of the linear and nonlinear optical properties of large varieties of GQDs (~400 systems) in size and topology utilizing the strengths of both semiempirical and first-principles methods. Our detailed study shows how the spectral shift and trends in the optical nonlinearity of GQDs depend on their structure, size, and shape. Among the circular, triangular, stripe, and random shaped GQDs, we find that GQDs with inequivalent sublattice atoms always possess lower HOMO−LUMO gap, broadband absorption, and high nonlinear optical coefficients. Also, we find that a majority of the GQDs with interesting linear and nonlinear optical properties have zigzag edges, although the reverse is not always true. We strongly believe that our findings can act as guidelines to design GQDs in optical parametric oscillators, higher harmonic generators, and optical modulators.

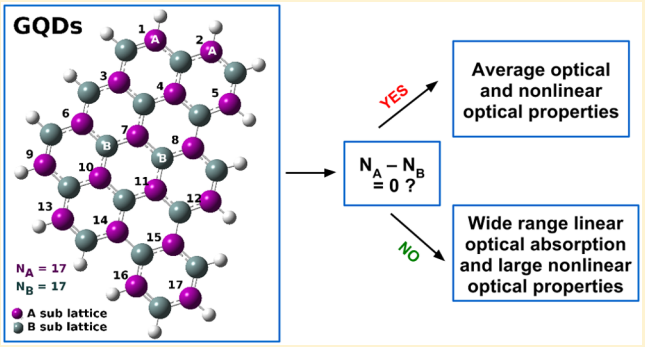

INTRODUCTION

Materials with broadband absorption (BBA) and emission, that is, covering ultraviolet, visible, and near-infrared regions of the solar spectrum, have important applications in photodetectors, broadband modulators, bioimaging, solar cells, etc.[1−6] Moreover, if the materials with the broadband absorption also show optical nonlinearity, they can be very useful in applications involving optical parametric oscillation, high harmonic generation,[7,8] Kerr effect,[9,10] and multiphoton imaging.[11] Thus, finding novel materials with both broadband absorption and optical nonlinear activity is of great interest.

Groups IV−VI quantum dots like CdSe, PbSe, CdS, HgTe, ZnSe, etc. have already been in a variety of applications involving light emitting diodes, bioimaging and solar cells because of their tunable absorption and specific optical nonlinear activity.[12−17] Materials prepared from high band gap semiconductors like ZnS, ZnSe, GaN, and AlN possess ultraviolet optical activity, whereas CdS and rare earth doped GaN materials exhibit near-IR activities.[18,19] Although tuning the size of a quantum dot can vary its active optical range, it cannot give the whole range altogether (i.e., simultaneous UV−vis and IR range activity). To this end, GQDs and modified GQDs seem to be promising materials for such optical activities.[20−23] Together with their higher photostability, biocompatibility, and low cost preparation, GQDs may act as a substitute for the toxic groups IV−VI quantum dots.

GQDs are the confined graphene materials available in various topologies,[20−25] and graphene is a layered sp^2-bonded carbon material in honeycomb lattice. Graphene with its zero band gap has a limitation to its applications in optoelectronics due to its zero optical emission. On the other hand, GQDs exhibit a broadband absorption and they have emerged as attractive fluorescence materials in the ultraviolet, visible, and even infrared regions.[20−23,26] During recent years, there has been a lot of research on the broadband activity of GQDs of different sizes, shapes, and functionalities through both experiment and theory.[27−31] Also, there is progress in identifying the shape and size dependent nonlinear activity of GQDs.[32−35]

Considering these studies, here, we have performed a systematic computational study on the linear and nonlinear optical (NLO) properties of hydrogen passivated GQDs (hence, may also be termed as polyaromatic hydrocarbons (PAHs)) of various sizes, shapes, edge structures, and so forth. After careful analysis of these GQDs (~20) with simultaneous BBA and high NLO coefficients, we find that the necessary and sufficient condition for possessing such multifunctionality is the presence of inequivalent sublattice atoms. Also, we find that a majority of the GQDs with only zigzag edges possess this

Received: April 13, 2015
Published: May 4, 2015

DOI: 10.1021/acs.jpcc.5b03531
J. Phys. Chem. C 2015, 119, 12079−12087

multifunctionality. Additionally, we find that some of these GQDs show fascinating first hyperpolarizabilities ($\sim 10^3-10^5$ times larger than the traditional NLO compounds [like *p*-nitroaniline, etc.]). In the following, first we have described how we have modeled our systems and then we have given the details of our computations. Next, we have compared the results from our semiempirical calculations on structural stability and electronic properties with the earlier studies and then we have presented our results on linear and nonlinear optical properties. Finally, we have presented the results from first-principles calculations on the systems, followed by the conclusions and possible extensions to the present work.

MODELING AND COMPUTATIONAL DETAILS

As the number of varieties of GQDs that can be generated from graphene is huge, following Kuc et al.[25] we have considered ~400 structures, based on their size, shape, edge, etc. As the hydrogen passivated GQDs have been shown to be more stable than the GQDs with bare edges, we have only considered the former ones throughout our study. As in ref 25, we have categorized our GQDs as circular (F) or triangular (T) or stripes (i.e., nanoribbons) (S) depending on their shape and zigzag (z) or armchair (a) depending on their edges. Thus, F_a (T_z) represents circular (triangular) GQDs with armchair (zigzag) edges. All other GQDs that do not fit in these categories mainly represent the different possible conformers of a GQD with particular number of carbon atoms, and we refer to them as random shaped GQDs. We identify these random shaped GQDs with their carbon atom numbers such as C22, C28, C74, etc. In Figure 1 we have shown typical examples of random shaped GQDs.

All the structural optimizations have been performed using self-consistent charge (SCC) density functional tight-binding (DFTB) theory[36] within third order expansion of the energy (DFTB3)[37] and with 3ob parameter set,[38] as implemented in DFTB+ package.[39] DFTB level of theory is used mainly because of the large number of systems (~400) considered in this study as well as its ability to give trends in band-gaps, energies, etc. which are comparable to the ones given by DFT, especially for carbon related materials, even with different edges, defects, etc.[40,41] Geometry optimizations have been performed using conjugate gradient method, and systems are considered to be optimized only when forces on all the atoms are less than 0.0001 Ha/bohr. For those systems whose energy levels near the Fermi-level are almost degenerate, we have increased the electronic temperature to 100 K to avoid any convergence issues.

Linear optical properties of all the compounds have been computed at the semiempirical ZINDO/S level of theory as implemented in Gaussian 09 software package.[42] ZINDO/S has been proved to be very successful especially in predicting the optical properties of systems containing C, N, O, H atoms like polyaromatic hydrocarbon compounds,[43,44] chlorophylls,[45] etc.[46] At a semiempirical level, nonlinear optical (NLO) properties of all compounds have been calculated using MOPAC2012 program package.[47,48] All the first-principles calculations for the linear (at time dependent density functional theory (TDDFT) level) and nonlinear optical properties have been performed using Gaussian 09. Long range corrected (CAM-B3LYP) exchange correlation functional has been used in conjunction with 6-31+g(d) basis set for all the calculations. A minimum of the first 12 lowest excited states have been considered in all the studies. GaussSum-2.2.6.1[49] is used to plot the absorption spectra, and a broadening of 0.333 eV has been used. To ensure the reliability of our calculations, we have compared our semiempirical and first-principles results on the linear and nonlinear optical properties of *p*-nitroaniline with its reported experimental values. We find that both the results are in close agreement (see Table S1 of Supporting Information (SI)).

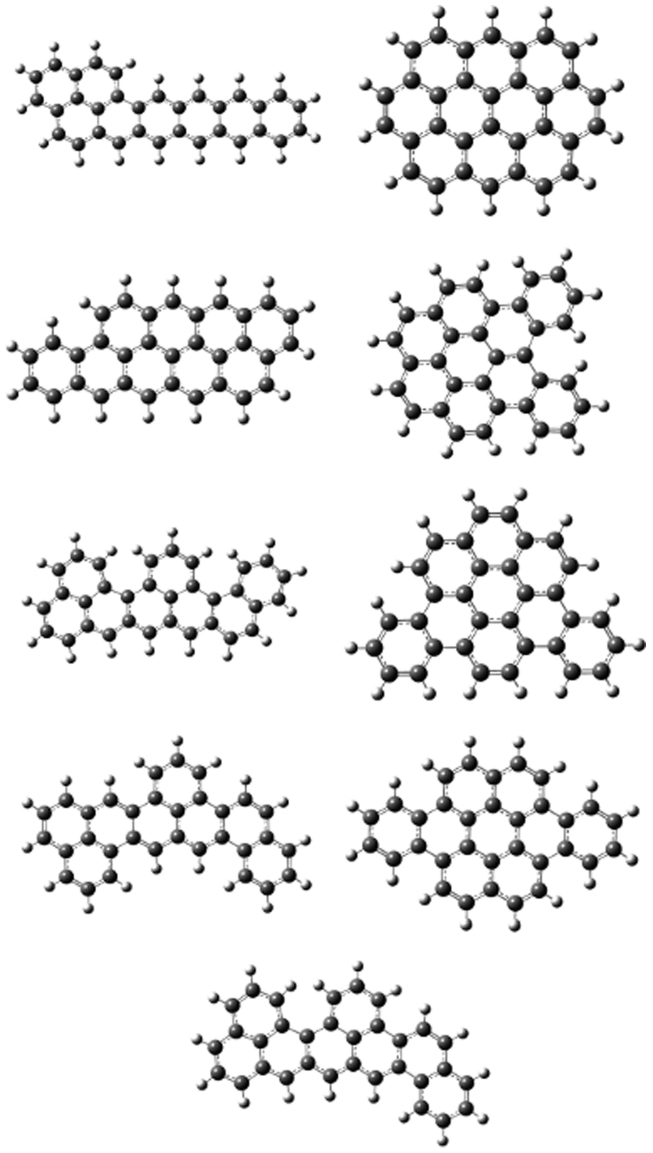

Figure 1. Some random shaped GQDs with 32 carbon atoms (C32).

RESULTS AND DISCUSSION

Energetic Stability and Electronic Properties. All the GQDs considered in this study are found to be energetically stable; that is, they have negative formation energy, $E_{Form} = E_{tot} - N_H E_H - N_C E_C$, where E_{tot}, E_H, and E_C are the total energy of the system, energy of the hydrogen atom in a H_2 molecule (i.e., $E_{H2}/2$), and energy of the carbon atom in a graphene lattice (i.e., E_{Graph}/N_C), respectively. Here, N_C and N_H are the number of carbon and hydrogen atoms in the system. At DFTB3 level of theory, we find E_H and E_C to be −9.123 and −44.291 eV, respectively. A plot of formation energy per atom vs $N_H/(N_H + N_C)$ of all the systems is given in Figure 2a. Clearly, there is a near linear relationship between the formation energy per atom

DOI: 10.1021/acs.jpcc.5b03531
J. Phys. Chem. C 2015, 119, 12079−12087

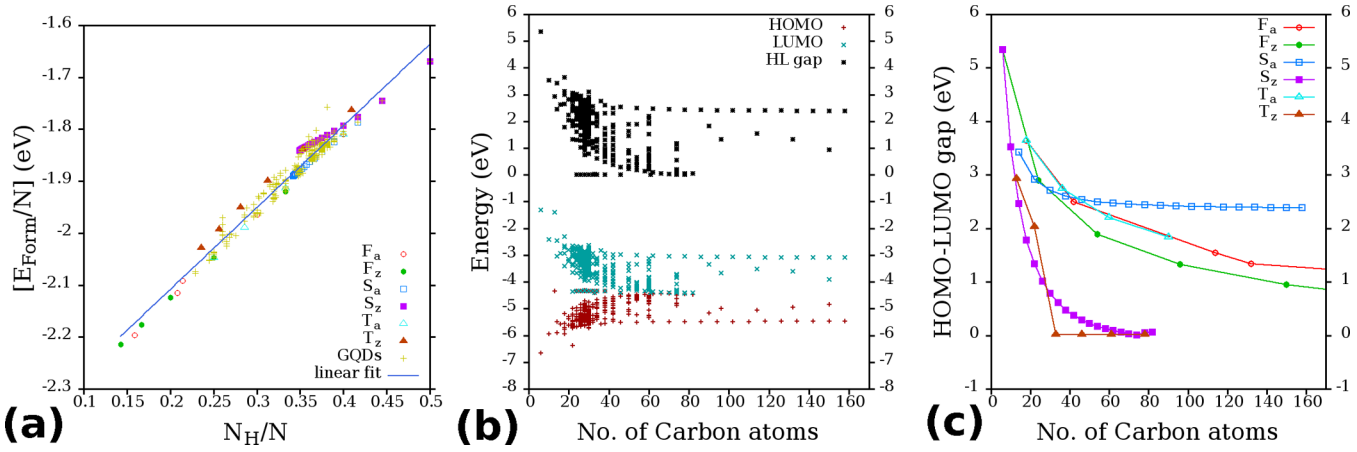

Figure 2. (a) Plot of E_{Form} per atom versus number of edge atoms to the total number of atoms (N) of all the GQDs. Straight line shows the linear fit. (b) Energies of HOMO, LUMO, and the HOMO − LUMO gap (HLG) of all the GQDs. (c) Changes in the HLG with size for different shaped GQDs. Symbols T, F, S represent triangular, circular, and striped GQDs. Subscripts a and z represent armchair and zigzag edges. See modeling section for further details.

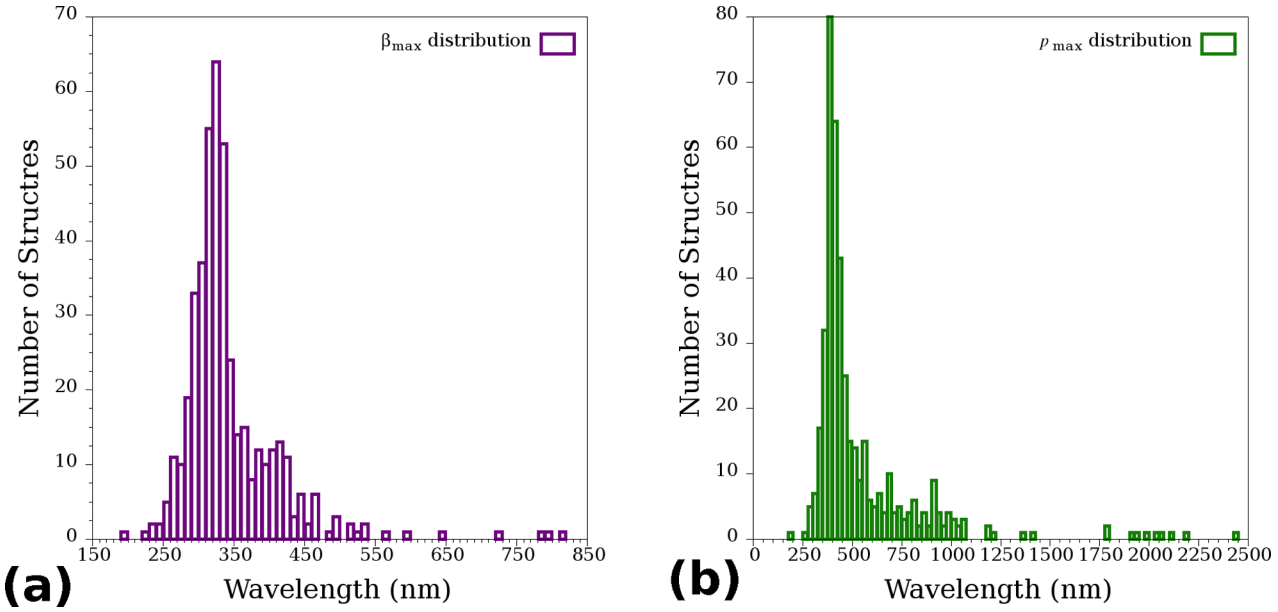

Figure 3. Histograms of wavelengths corresponding to (a) β_{max} and (b) p_{max} excitation in all GQDs. p_{max} excitations above 2500 nm have been omitted for clarity.

and the number of edge atoms in all the systems (notice the linear fit in Figure 2a); that is, system with lesser number of edge atoms is easier to form and vice versa, as expected.[20,50,51] Similar results have been observed in some of the earlier studies on GQDs and PAHs.[25,52] In agreement with these previous studies, we also find that among the different GQD shapes studied here, circular GQDs are the most stable ones and ribbon-like GQDs are the least stable. The stability of all other GQDs (triangular, random, etc.) falls between these two types of GQDs [see Figure 2a]. The reason for such a trend is again due to the less number of edge atoms in circular GQDs than in other GQDs considered in this study, as evident from the x-axis of Figure 2a. Recent molecular dynamics simulations have also shown that among the different GQDs, circular and triangular GQDs with zigzag edges are the most stable ones until ∼4000 K.[24]

Next, the energies of HOMO, LUMO, and their difference (i.e., HOMO − LUMO gap (HLG)) of all the GQDs are plotted in Figure 2b as a function of number of carbon atoms. The calculated HLG values are mainly in the range of ∼0−3 eV. Also, from Figure 2b and Figure 2c, it can be observed that for a particular N_C, one can tune the HLG from ∼0−3 eV depending on the shape and edges of the GQD. Indeed, tuneability of band gap between ∼0 and 3 eV has already been reported for armchair graphene nanoribbons by varying their width[53,54] and for the case of GQDs by varying their shape.[22,23,55,56] Interestingly, we find that such tuning is possible even for the systems with N_C between 20 to 50. In fact, synthesis of GQDs (actually, PAHs) of different sizes have already been carried out.[21] From Figure 2c, it can be noted that HLGs of the systems with zigzag edges converge rapidly to zero (reaching the semimetallicity of graphene) compared with the armchair ones, irrespective of the shapes, and the calculated trend of convergence is T_z-GQDs > S_z-GQDs > F_z-GQDs > T_a-GQDs ∼ F_a-GQDs > S_a-GQDs. As HLG reflects the kinetic stability of a system, the above trends suggest that kinetic

DOI: 10.1021/acs.jpcc.5b03531
J. Phys. Chem. C 2015, 119, 12079−12087

stability will be highest for S_a-GQDs and least for T_z-GQDs and S_z-GQDs. As suggested by the Clar's rule,[21] higher kinetic stability of S_a-GQDs, compared to the other structures, is due to the presence of a larger number of resonant sextets in these structures. Similar reasons are also known for the lesser stability of zigzag edged structures compared to the armchair ones.[25] One may also note that the HLG of "S_z and T_z", "T_a and F_a"-GQDs follows a similar trend as N_C increases (for $N_C > 60$), as has also been observed in some of the recent studies.[24] Finally, as the HLG of these GQDs are tunable over a wide range and as HLG can be used as a rough estimate for the optical gap,[43] one may immediately expect that the optical properties of these GQDs can also be tuned over a wide range, and the results of the respective calculations are given below.

Optical Properties. First, we present the optical absorption of all the systems calculated at the ZINDO/S level of theory. Here, we have analyzed only the 20 low energy singlet excitations from the ZINDO/S results. Absorption spectra of PAHs mainly consist of three bands, namely, alpha (α), beta (β), and para (p), out of which the most intense ones are β and p-bands (notations are according to Clar's rule,[21] where p(β)-bands correspond to the bands at higher (lower) wavelengths). Interestingly, in a very recent study[43] it has been concluded that ZINDO/S is good at predicting the most intense p and β bands of all $C_{32}H_{16}$ benzenoid PAHs. Considering these facts, first we have plotted the histograms of "wavelengths corresponding to the most intense p-bands (p_{max}) and β-bands (β_{max})", respectively, in Figures 3a and Figure 3b and the corresponding oscillator strengths (OS) histograms in Figure S1a and Figure S1b. From these figures it can be noted that a majority of the systems have their β_{max} and p_{max} in the UV−vis region (200−760 nm) and the oscillator strength of β_{max} (p_{max}) is almost always (for majority of structures) >0.5 (0.1). Thus, a majority of GQDs considered in this study absorb strongly in the UV−vis region (in particular, their β_{max} (p_{max}) is located in the region between 250 and 450 (300−700) nm).

However, interestingly, we find ∼70 GQDs whose p_{max} is in the IR region (>760 nm). Materials absorbing in the IR region are of great interest in the preparation of solar cells because half of the solar energy received by earth is in IR radiation range and most of the present day solar cells do not utilize this energy region.[20] Thus, knowing the reason for the IR activity of these GQDs will be of great use, and for this we have analyzed their p_{max} transition. In Table S1, we have given the calculated wavelength, OS, and the major contributions of the molecular orbitals corresponding to the p_{max} transition for all the IR-active GQDs. Clearly, p_{max} transition always has the major contributions from excitations involving the frontier orbitals (that is, HOMO − 1, HOMO, LUMO, and LUMO + 1), especially from HOMO and LUMO. Thus, the changes in these frontier MOs lead to changes in the p_{max} transition. Also, some of the earlier studies on PAHs have found that HLG of these systems is almost equal to the energy corresponding to the p_{max} transition (see ref 43 and references therein).

For a few of these GQDs, we find HLG to be very small. In general, small HLGs occur either because of extended delocalization (as in conjugated carbon chains) or if there exists a lesser number of resonant sextets (according to Clar's rule[21,25,43]). In our case, however, the very small HLGs are seen because of completely different reasons. If we look at the structures of these GQDs closely, we find that they do not have the same number of sublattice atoms (i.e., $N_A - N_B \neq 0$). In fact, in all the random shaped GQDs, we find there exist two additional sublattice atoms of one type (i.e., $|N_A - N_B| = 2$). p_z orbitals of these additional atoms remain as nonbonding orbitals and appear at the zero of energy (i.e., at the Fermi level) in the energy level diagram. If there were no interactions (as in tight-binding calculations), both of these levels would be degenerate and would appear exactly at the zero of energy (similar to what has been observed in triangular GQDs[22,23,57−59]). However, because of interaction terms in ZINDO/S Hamiltonian, we find the two levels to appear above and below the zero of energy with a very low energy gap (few meV). Interestingly, these two levels have opposite parity due to which the transition dipole moment between the two become nonzero. Thus, these two levels give rise to optical transition with a finite oscillator strength (OS). Since the energy gap between these two levels is too small, the optical absorption appears in the IR region.

As an example, in Figure 4a−d we have given four structural isomers (hereafter addressed as 4a, 4b, 4c and 4d, respectively)

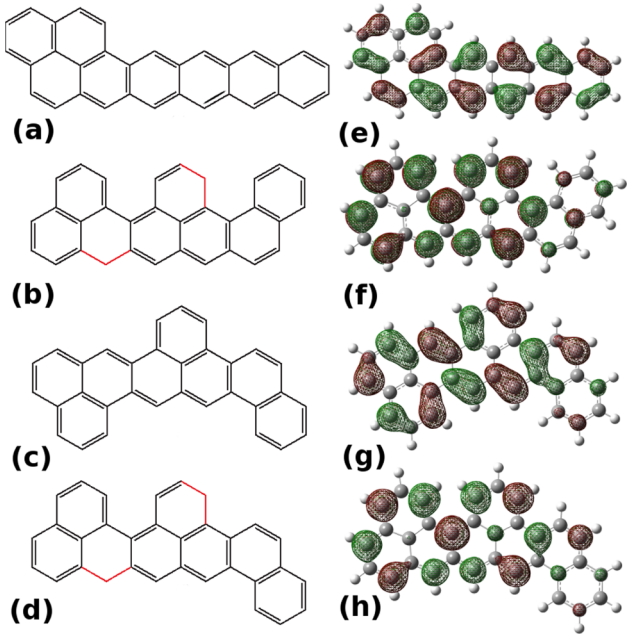

Figure 4. Schematic diagrams of four structural isomers of $C_{32}H_{18}$ GQD (a−d) and their HOMO isosurfaces (e−h), respectively. Isovalue of 0.02 e/Å ^{3} is used for all the plots.

of $C_{32}H_{18}$, where only 4b and 4d have the sublattice imbalance. As explained, for 4b and 4d only, we find p_{max} in the IR region (>2000 nm) but not for 4a and 4c. In Figure 4, we have also given the conjugation and isosurface plots of HOMO for these GQDs. As can be seen, because of sublattice imbalance, the conjugation in 4b and 4d GQDs is not continuous and there are "conjugation breaks", which are a clear demonstration of solitonic structure (conjugated system) and domain walls (seen in ferromagnetic metal blocks). The main point is that these defect states are intrinsic in these GQDs and these have not been externally induced.

IR activity of GQDs that absorb below 2500 nm is mainly due to the zigzag edge nature of these GQDs, which lowers their HLG. For example, it is well-known that the polyacenes have the lowest HLG among the various PAHs[21] and p_{max} of hexacene (six fused benzne rings) itself is 750 nm. Also, Hod et al.[53,54] have shown that rectangular GQDs can possess low HLG, and through TDDFT calculations, our group has also

DOI: 10.1021/acs.jpcc.5b03531
J. Phys. Chem. C 2015, 119, 12079−12087

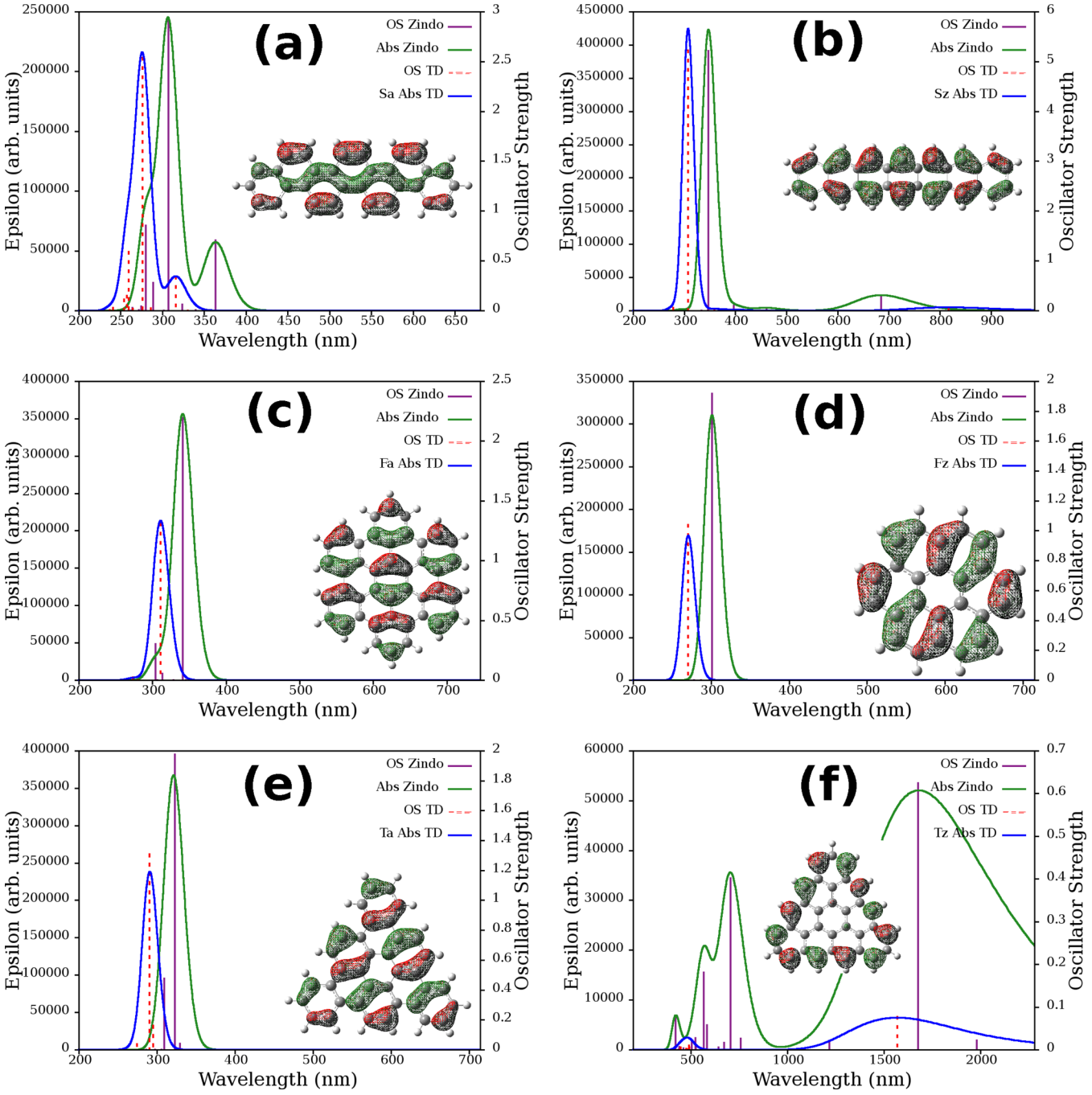

Figure 5. Absorption profiles of GQDs of various shapes calculated at both ZINDO/S level of theory and using TDDFT at CAMB3LYP/6-31+g(d) level of theory. Insets in each part show the isosurface of the HOMO of that GQD calculated using TDDFT. (a)−(f) represent S_a, S_z, F_a, F_z, T_a, and T_z GQDs, respectively. Isovalue of 0.02 e/Å ^{3} is used for all the plots.

shown that p_{max} of rectangular GQDs is ∼1900 nm.[20] Inspecting the structures of GQDs that absorb in the region of 760−2500 nm, we find that all these GQDs have either polyacene type structure or rectangular type structure, with some of their edges being substituted with ethene, propene, *cis*-1,3-dibutene, etc. (see Figure S3). Also, it is important to mention that HOMO of all the IR-active structures is different from that of the non-IR-active structures.

Frontier MOs of IR-active GQDs have larger number of nodes and hence look like the collection of p_z orbitals on individual carbon atoms without overlap (for example, see Figure 4f and Figure 4h). The reverse is true for the non-IR-active GQDs (see Figure 4e and Figure 4g). Presence of a large number of nodes destabilizes HOMO compared to its structural isomers with less number of nodes and hence lesser HLG and IR activity. As an example of the above-mentioned observations, we have given absorption spectra and isosurfaces of HOMO of C32 and C74 GQDs in Figures S2−S4. Finally, as the OS of the p_{max} peak for a majority of these GQDs is >0.5 and as the OS of the β_{max} peak is almost always found to >0.5, we find that these GQDs can have broadband absorption (BBA), as predicted earlier for triangular GQDs[22,23] and rectangular GQDs.[20] BBA of these GQDs can also be seen in Figures S2 and S4. To conclude all of the above results, we find

DOI: 10.1021/acs.jpcc.5b03531
J. Phys. Chem. C 2015, 119, 12079−12087

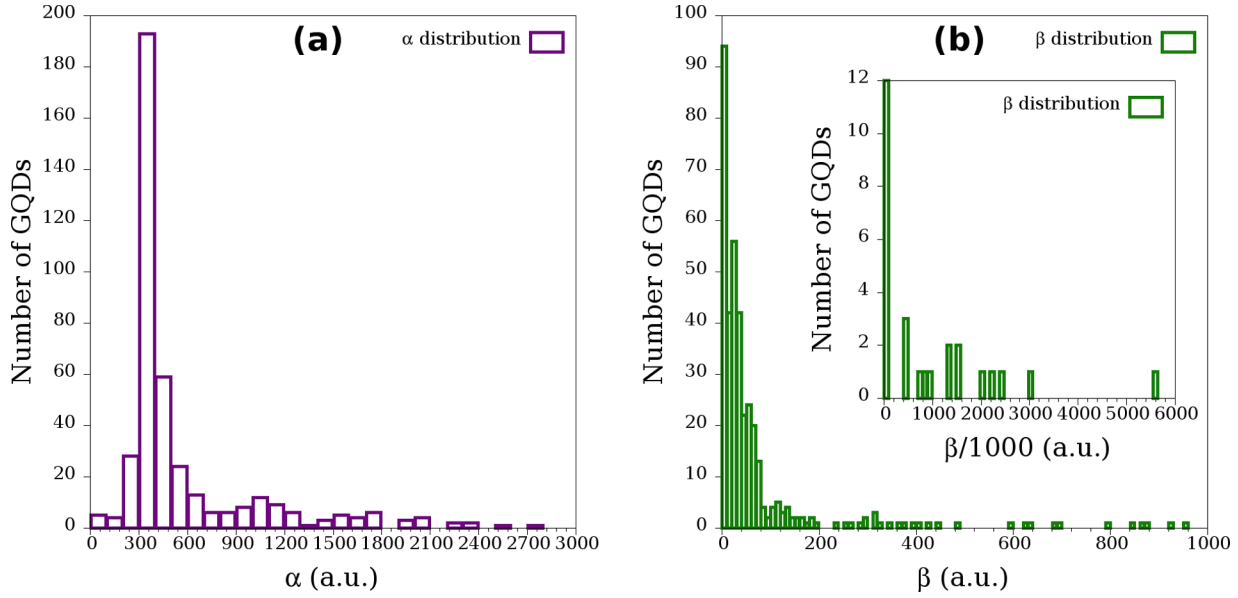

Figure 6. Histograms of isotropic average values of (a) polarizability α and (b) first hyperpolarizability β of all GQDs.

that GQDs with inequivalent sublattice atoms or GQDs with rectangular or stripe shapes can absorb in the IR region and they may be suitable candidates for BBA.

To put the results obtained from the ZINDO/S method on a solid footing, we have performed TDDFT calculations at CAMB3LYP/6-31+g(d) level of theory on a few GQDs. First, we will present our results on GQDs of various shapes. In Figure 5a–f, we have given the absorption spectra of S_a, S_z, F_a, F_z, T_a, and T_z, respectively, calculated at both ZINDO/S and TDDFT levels of theory along with the isosurfaces of their HOMO (only from TDDFT). Clearly, absorption profiles of both methods compare farily well, although OS values predicted by ZINDO/S are higher than that of TDDFT. Also, λ_{max} predicted by ZINDO/S is consistently red-shifted compared to the TDDFT predicted values. Consistent with the previous arguments on the isosurface of HOMO (calculated using ZINDO/S), even with TDDFT we find a larger number of nodes (see Figure 5f) in the HOMO if the GQD has IR activity and it has more overlapping character if the GQD is not IR-active (see Figure 5a–e). Also, we find that the character of the p_{max} excitation (i.e., MOs involved in the excitation) is similar in both methods. Importantly, we find that GQDs whose HOMO is mainly localized on the edge atoms (as in S_z and T_z) and whose p_{max} excitation has major contribution from HOMO to LUMO are IR-active. From Figure 5, one may also infer that the presence of zigzag edges is only a necessary but not a sufficient condition (example being the F_z GQDs) for the IR absorption. Finally, to see the effect of inequivalent sublattice atoms on the IR activity, we have considered five C28-GQDs with $N_A - N_B = 2$, and we find all of them to be IR-active, again consistent with the ZINDO/S results (see Table S2). Thus, we find that results of ZINDO/S and TDDFT are consistent and compare well for the GQDs considered in this study.

Nonlinear Optical Properties. In this section, we present the linear polarizability (α) and first hyperpolarizability (β) of all the GQDs calculated using the finite field approach as implemented in the MOPAC and Gaussian 09 packages. Expressions for the dipole moment and the energy of a molecule interacting with an external electric field are given by eqs 1 and 2.[60]

$$\mu_i = \mu_{0i} + \alpha_{ij}F_j + \frac{1}{2}\beta_{ijk}F_jF_k + \frac{1}{6}\gamma_{ijkl}F_jF_kF_l + \ldots \quad (1)$$

$$E(F) = E(0) - \mu_iF_i - \frac{1}{2!}\alpha_{ij}F_iF_j - \frac{1}{3!}\beta_{ijk}F_jF_k - \frac{1}{4!}\gamma_{ijkl}F_jF_kF_l - \ldots \quad (2)$$

where μ_0 is the permanent dipole moment and α_{ij}, β_{ijk}, and γ_{ijkl} are the linear polarizability and first and second hyperpolarizability tensor elements, respectively. Also, for a molecule, the average values of above quantities (μ_{av}, etc.) are defined as

$$\mu_{av} = (\mu_x^2 + \mu_y^2 + \mu_z^2)^{1/2} \quad (3)$$

$$\alpha_{av} = \frac{1}{3}(\alpha_{xx} + \alpha_{yy} + \alpha_{zz}) \quad (4)$$

$$\beta_{av} = (\beta_x^2 + \beta_y^2 + \beta_z^2)^{1/2} \quad (5)$$

where

$$\beta_i = \frac{3}{5}(\beta_{iii} + \beta_{ijj} + \beta_{ikk}); \quad i, j, k = x, y, z \quad (6)$$

In Figure 6a and Figure 6b, we have plotted the distribution of isotropic average α and β values for all the GQDs at static field. Similar to absorption profiles, a majority of the GQDs' α and β values are confined to a small region. For these majority GQDs, we find that the α and β values are in the range of 250–700 au (~40–100 Å ^{3}) and 1–200 au (10^{-32}–10^{-30} esu), respectively. Compared to the α and β values of *p*-nitroaniline (16.346 and 978.21 au, respectively), it is nice to note that a majority of the GQDs already have high polarizability and moderate hyperpolarizabilities. Importantly, we find that several GQDs possess α and β values that are orders of magnitude greater than that of *p*-nitroaniline (see Figure 6a and inset of Figure 6b).

In general, both linear polarizability and first order hyperpolarizabilities have an inverse relationship with the

DOI: 10.1021/acs.jpcc.5b03531
J. Phys. Chem. C 2015, 119, 12079–12087

energy gap between the states involved in the polarization and are directly proportional to the transition moment. Thus, we can expect an increase in α and β if the ground and excited states are closely spaced or the transition moment between the states is high or both. From the above reasoning, one can also infer that GQDs with low HLG and whose first excited state has major contribution from HOMO to LUMO transition should give higher α and β values. Indeed, we find that all the GQDs that are IR-active also have high α and β (except the GQDs with inversion symmetry) values, that is, above the ranges of 250−700 au and 1−200 au, respectively. Also, we find that some of the GQDs with zigzag edges, like F_z, which are not IR-active but have very high oscillator strength for the p_{max} (see Figure 5d) excitation, also show higher α values. However, because of the presence of inversion symmetry, such GQDs do not have higher β values. Finally, we again find that trends in our results from semiempirical calculations compare farily well with that of first-principles calculations (see Table S4). On the basis of all the above results, we conjecture that GQDs with very low HLGs can have both broadband absorption and nonlinear optical activity and hence are potential candidates for optoelectronic devices.

CONCLUSIONS

We have performed a systematic study on the GQDs of various sizes, shapes, and edges to explore their linear and nonlinear optical properties. First, we find the formation energies of GQDs have a near linear dependence on their number of edge atoms and HOMO − LUMO gaps of a GQD with a particular number of carbon atoms can be tuned from ∼0 to 3 eV depending on its shape and edge nature. Trends in the HLG can be understood based on the Clar's rule of aromatic sextets for majority of the sytems. Extremely low HLGs of certain GQDs are due to the presence of unequal number of sublattice atoms in these GQDs, that is, $N_A - N_B \neq 0$. Tunability of HLG has also been reflected in the tunability of the absorption profiles in these GQDs. We find that a majority of the GQDs absorb strongly in the UV−vis region with their β_{max} (p_{max}) being located in the region between 250 and 450 (300−700) nm), and their α and β values are in the ranges of 250−700 au and 1−200 au, respectively. However, ∼70 GQDs have their p_{max} in the IR region and have higher α (>700 au) and β (>200 au) values. A common feature that we find in all these IR-active GQDs is the existence of a larger number of nodes in the isosurface of HOMO which leads to an increment in HOMO energy and hence decrement in the HLG. Because of their high oscillator strengths in both UV−vis and IR regions, these GQDs can possess broadband absorption. With their high α and β values along with the BBA, we expect them to be potential candidates for optoelectronic devices.

ASSOCIATED CONTENT

Supporting Information

Table containing the wavelength, OS and MO contributions to the p_{max} transition for the GQDs with p_{max} in IR-region; absorption spectra and isosurfaces of HOMO for C32 and C74 GQDs; comparison of ZINDO/s results with TDDFT and experimental results. The Supporting Information is available free of charge on the ACS Publications website at DOI: 10.1021/acs.jpcc.5b03531.

AUTHOR INFORMATION

Corresponding Author

*E-mail: pati@jncasr.ac.in.

Notes

The authors declare no competing financial interest.

ACKNOWLEDGMENTS

S.S.R.K.C.Y., M.M., and S.K.P. acknowledge TUE-CMS, JNCASR for the computational facilities and DST for funding. S.S.R.K.C.Y. thanks Dr. Noel for his help in GaussSum.

REFERENCES

(1) Zheng, J.; Barton, R. a.; Englund, D. Broadband Coherent Absorption in Chirped-Planar-Dielectric Cavities for 2D-Material-Based Photovoltaics and Photodetectors. *ACS Photonics* **2014**, *1*, 768−774.

(2) Sun, H.; Autschbach, J. Electronic Energy Gaps for π-Conjugated Oligomers and Polymers Calculated with Density Functional Theory. *J. Chem. Theory Comput.* **2014**, *10*, 1035−1047.

(3) Kim, J. T.; Yu, Y.-J.; Choi, H.; Choi, C.-G. Graphene-Based Plasmonic Photodetector for Photonic Integrated Circuits. *Opt. Express* **2014**, *22*, 803−808.

(4) Sobon, G.; Sotor, J.; Pasternak, I.; Strupinski, W.; Krzempek, K.; Kaczmarek, P.; Abramski, K. M. Chirped Pulse Amplification of a Femtosecond Er-Doped Fiber Laser Mode-Locked by a Graphene Saturable Absorber. *Laser Phys. Lett.* **2013**, *10*, 035104.

(5) Urich, A.; Unterrainer, K.; Mueller, T. Intrinsic Response Time of Graphene Photodetectors. *Nano Lett.* **2011**, *11*, 2804−2808.

(6) Sun, Z.; Hasan, T.; Torrisi, F.; Popa, D.; Privitera, G.; Wang, F.; Bonaccorso, F.; Basko, D. M.; Ferrari, A. C. Graphene Mode-Locked Ultrafast Laser. *ACS Nano* **2010**, *4*, 803−810.

(7) Sørngård, S. A.; Simonsen, S. I.; Hansen, J. P. High-Order Harmonic Generation from Graphene: Strong Attosecond Pulses with Arbitrary Polarization. *Phys. Rev. A* **2013**, *87*, 053803.

(8) Hong, S.-Y.; Dadap, J. I.; Petrone, N.; Yeh, P.-C.; Hone, J.; Osgood, R. M. Optical Third-Harmonic Generation in Graphene. *Phys. Rev. X* **2013**, *3*, 021014.

(9) Shen, T.-Z.; Hong, S.-H.; Song, J.-K. Electro-Optical Switching of Graphene Oxide Liquid Crystals with an Extremely Large Kerr Coefficient. *Nat. Mater.* **2014**, *13*, 394−399.

(10) Shimano, R.; Yumoto, G.; Yoo, J. Y.; Matsunaga, R.; Tanabe, S.; Hibino, H.; Morimoto, T.; Aoki, H. Quantum Faraday and Kerr Rotations in Graphene. *Nat. Commun.* **2013**, *4*, 1841.

(11) Yang, H.; Feng, X.; Wang, Q.; Huang, H.; Chen, W.; Wee, A. T. S.; Ji, W. Giant Two-Photon Absorption in Bilayer Graphene. *Nano Lett.* **2011**, *11*, 2622−2627.

(12) Mashford, B. S.; Stevenson, M.; Popovic, Z.; Hamilton, C.; Zhou, Z.; Breen, C.; Steckel, J.; Bulovic, V.; Bawendi, M.; Coe-Sullivan, S.; Kazlas, P. T. High-Efficiency Quantum-Dot Light-Emitting Devices with Enhanced Charge Injection. *Nat. Photonics* **2013**, *7*, 407−412.

(13) Klimov, V.; Mikhailovsky, A.; Xu, S. Optical Gain and Stimulated Emission in Nanocrystal Quantum Dots. *Science* **2000**, *290*, 314−318.

(14) Choi, H.; Radich, J. G.; Kamat, P. V. Sequentially Layered CdSe/CdS Nanowire Architecture for Improved Nanowire Solar Cell Performance. *J. Phys. Chem. C* **2014**, *118*, 206−213.

(15) Tian, J.; Liu, R.; Zhao, Y.; Peng, Y.; Hong, X.; Xu, Q.; Zhao, S. Synthesis of CdTe/CdS/ZnS Quantum Dots and Their Application in Imaging of Hepatocellular Carcinoma Cells and Immunoassay for Alpha Fetoprotein. *Nanotechnology* **2010**, *21*, 305101.

(16) Somers, R. C.; Bawendi, M. G.; Nocera, D. G. CdSe Nanocrystal Based Chem-/Bio- Sensors. *Chem. Soc. Rev.* **2007**, *36*, 579−591.

(17) Lad, A. D.; Prem Kiran, P.; Ravindra Kumar, G.; Mahamuni, S. Three-Photon Absorption in ZnSe and ZnSeZnS Quantum Dots. *Appl. Phys. Lett.* **2007**, *90*, 133113.

DOI: 10.1021/acs.jpcc.5b03531
J. Phys. Chem. C 2015, 119, 12079−12087

(18) Shavel, A.; Gaponik, N.; Eychmüller, A. Efficient UV-Blue Photoluminescing Thiol-Stabilized Water-Soluble Alloyed ZnSe(S) Nanocrystals. *J. Phys. Chem. B* **2004**, *108*, 5905−5908.
(19) Dennis, A. M.; Mangum, B. D.; Piryatinski, A.; Park, Y.-S.; Hannah, D. C.; Casson, J. L.; Williams, D. J.; Schaller, R. D.; Htoon, H.; Hollingsworth, J. a. Suppressed Blinking and Auger Recombination in Near-Infrared Type-II InP/CdS Nanocrystal Quantum Dots. *Nano Lett.* **2012**, *12*, 5545−5551.
(20) Yamijala, S. S.; Bandyopadhyay, A.; Pati, S. K. Structural Stability, Electronic, Magnetic, and Optical Properties of Rectangular Graphene and Boron Nitride Quantum Dots: Effects of Size, Substitution, and Electric Field. *J. Phys. Chem. C* **2013**, *117*, 23295−23304.
(21) Rieger, R.; Müllen, K. Forever Young: Polycyclic Aromatic Hydrocarbons as Model Cases for Structural and Optical Studies. *J. Phys. Org. Chem.* **2010**, *23*, 315−325.
(22) Güçlü, A.; Potasz, P.; Korkusinski, M.; Hawrylak, P. *Graphene Quantum Dots*; NanoScience and Technology; Springer: Heidelberg, Germany, 2014.
(23) Güçlü, a. D.; Potasz, P.; Hawrylak, P. Excitonic Absorption in Gate-Controlled Graphene Quantum Dots. *Phys. Rev. B* **2010**, *82*, 155445.
(24) Silva, a. M.; Pires, M. S.; Freire, V. N.; Albuquerque, E. L.; Azevedo, D. L.; Caetano, E. W. S. Graphene Nanoflakes: Thermal Stability, Infrared Signatures, and Potential Applications in the Field of Spintronics and Optical Nanodevices. *J. Phys. Chem. C* **2010**, *114*, 17472−17485.
(25) Kuc, A.; Heine, T.; Seifert, G. Structural and Electronic Properties of Graphene Nanoflakes. *Phys. Rev. B* **2010**, *81*, 085430.
(26) Sk, M. A.; Ananthanarayanan, A.; Huang, L.; Lim, K. H.; Chen, P. Revealing the Tunable Photoluminescence Properties of Graphene Quantum Dots. *J. Mater. Chem. C* **2014**, *2*, 6954.
(27) Fang, Z.; Wang, Y.; Schlather, A.; Liu, Z. Active Tunable Absorption Enhancement with Graphene Nanodisk Arrays. *Nano Lett.* **2013**, *14*, 299−304.
(28) Yan, X.; Li, B.; Li, L.-s. Colloidal Graphene Quantum Dots with Well-Defined Structures. *Acc. Chem. Res.* **2013**, *46*, 2254−2262.
(29) Tang, L.; Ji, R.; Li, X.; Bai, G.; Liu, C. P.; Hao, J.; Lin, J.; Jiang, H.; Teng, K. S.; Yang, Z.; Lau, S. P. Deep Ultraviolet to Near-Infrared Emission and Photoresponse in Layered N-Doped Graphene Quantum Dots. *ACS Nano* **2014**, *8*, 6312−6320.
(30) Riesen, H.; Wiebeler, C.; Schumacher, S. Optical Spectroscopy of Graphene Quantum Dots: The Case of C132. *J. Phys. Chem. A* **2014**, *118*, 5189−5195.
(31) Ozfidan, I.; Korkusinski, M.; Güçlü, A. D.; McGuire, J. A.; Hawrylak, P. Microscopic Theory of the Optical Properties of Colloidal Graphene Quantum Dots. *Phys. Rev. B* **2014**, *89*, 085310.
(32) Zhou, Z.; Liu, Z.; Li, Z. Shape Effect of Graphene Quantum Dots on Enhancing Second-Order Nonlinear Optical Response and Spin Multiplicity in NH2-GQD-NO2 Systems. *J. Phys. Chem. C* **2011**, 16282−16286.
(33) Yoneda, K.; Nakano, M.; Kishi, R.; Takahashi, H.; Shimizu, A.; Kubo, T.; Kamada, K.; Ohta, K.; Champagne, B.; Botek, E. Third-Order Nonlinear Optical Properties of Trigonal, Rhombic and Bow-Tie Graphene Nanoflakes with Strong Structural Dependence of Diradical Character. *Chem. Phys. Lett.* **2009**, *480*, 278−283.
(34) Yoneda, K.; Nakano, M.; Fukuda, K.; Champagne, B. The Odd Electron Density Is the Guide toward Achieving Organic Molecules with Gigantic Third-Order Nonlinear Optical Responses. *J. Phys. Chem. Lett.* **2012**, *3*, 3338−3342.
(35) Yoneda, K.; Nakano, M.; Inoue, Y. Impact of Antidot Structure on the Multiradical Characters, Aromaticities, and Third-Order Nonlinear Optical Properties of Hexagonal Graphene Nanoflakes. *J. Phys. Chem. C* **2012**, *116*, 17787−17795.
(36) Elstner, M.; Porezag, D.; Jungnickel, G.; Elsner, J.; Haugk, M.; Frauenheim, T.; Suhai, S.; Seifert, G. Self-Consistent-Charge Density-Functional Tight-Binding Method for Simulations of Complex Materials Properties. *Phys. Rev. B* **1998**, *58*, 7260.
(37) Yang, Y.; Yu, H.; York, D.; Cui, Q.; Elstner, M. Extension of the Self-Consistent-Charge Density-Functional Tight-Binding Method: Third-Order Expansion of the Density Functional Theory Total Energy and Introduction of a Modified Effective Coulomb Interaction. *J. Phys. Chem. A* **2007**, *111*, 10861−10873.
(38) Gaus, M.; Goez, A.; Elstner, M. Parametrization and Benchmark of DFTB3 for Organic Molecules. *J. Chem. Theory Comput.* **2013**, *9*, 338−354.
(39) Aradi, B.; Hourahine, B.; Frauenheim, T. DFTB+, a Sparse Matrix-Based Implementation of the DFTB Method. *J. Phys. Chem. A* **2007**, *111*, 5678−5684.
(40) Zobelli, A.; Ivanovskaya, V.; Wagner, P.; Suarez-Martinez, I.; Yaya, A.; Ewels, C. P. A Comparative Study of Density Functional and Density Functional Tight Binding Calculations of Defects in Graphene. *Phys. Status Solidi B* **2012**, *249*, 276−282.
(41) Enyashin, A. N.; Ivanovskii, A. L. Graphene Allotropes. *Phys. Status Solidi B* **2011**, *248*, 1879−1883.
(42) Frisch, M. J.; et al. *Gaussian 09*, revision B.01; Gaussian Inc.: Wallingford, CT, 2009.
(43) Oña Ruales, J. O.; Ruiz-Morales, Y. The Predictive Power of the Annellation Theory: The Case of the $C_{32}H_{16}$ Benzenoid Polycyclic Aromatic Hydrocarbons. *J. Phys. Chem. A* **2014**, *118*, 5212−5227.
(44) Cocchi, C.; Prezzi, D.; Ruini, A. Anisotropy and Size Effects on the Optical Spectra of Polycyclic Aromatic Hydrocarbons. *J. Phys. Chem. A* **2014**, *118*, 6507−6513.
(45) Linnanto, J.; Korppi-Tommola, J. Spectroscopic Properties of Mg-Chlorin, Mg-Porphin and Chlorophylls a, b, c1, c2, c3 and d Studied by Semi-Empirical and ab Initio MO/CI Methods. *Phys. Chem. Chem. Phys.* **2000**, *2*, 4962−4970.
(46) Voityuk, A. A. Intermediate Neglect of Differential Overlap for Spectroscopy. *WIREs Comput. Mol. Sci.* **2013**, *3*, 515−527.
(47) Stewart, J. J. P. *MOPAC2012*, version 14.212L; Stewart Computational Chemistry: Colorado Springs, CO; http://OpenMOPAC.net.
(48) Maia, J. D. C.; Urquiza Carvalho, G. A.; Mangueira, C. P.; Santana, S. R.; Cabral, L. A. F.; Rocha, G. B. GPU Linear Algebra Libraries and GPGPU Programming for Accelerating MOPAC Semiempirical Quantum Chemistry Calculations. *J. Chem. Theory Comput.* **2012**, *8*, 3072−3081.
(49) O'Boyle, N. M.; Tenderholt, A. L.; Langner, K. M. CCLIB: A Library for Package-Independent Computational Chemistry Algorithms. *J. Comput. Chem.* **2008**, *29*, 839−845.
(50) Yamijala, S. S.; Bandyopadhyay, A.; Pati, S. K. Electronic Properties of Zigzag, Armchair and Their Hybrid Quantum Dots of Graphene and Boron-Nitride with and without Substitution: A DFT Study. *Chem. Phys. Lett.* **2014**, *603*, 28−32.
(51) Bandyopadhyay, A.; Yamijala, S. S. R. K. C.; Pati, S. K. Tuning the Electronic and Optical Properties of Graphene and Boron-Nitride Quantum Dots by Molecular Charge-Transfer Interactions: A Theoretical Study. *Phys. Chem. Chem. Phys.* **2013**, *15*, 13881−13887.
(52) Fthenakis, Z. G. Energetics of Graphene Flakes. *Mol. Phys.* **2013**, *111*, 3289−3296.
(53) Barone, V.; Hod, O.; Peralta, J. E.; Scuseria, G. E. Accurate Prediction of the Electronic Properties of Low-Dimensional Graphene Derivatives Using a Screened Hybrid Density Functional. *Acc. Chem. Res.* **2011**, *44*, 269−279.
(54) Hod, O.; Barone, V.; Scuseria, G. E. Half-Metallic Graphene Nanodots: A Comprehensive First-Principles Theoretical Study. *Phys. Rev. B* **2008**, *77*, 035411.
(55) Kosimov, D. P.; Dzhurakhalov, a. a.; Peeters, F. M. Carbon Clusters: From Ring Structures to Nanographene. *Phys. Rev. B* **2010**, *81*, 195414.
(56) Zhang, Z. Z.; Chang, K.; Peeters, F. M. Tuning of Energy Levels and Optical Properties of Graphene Quantum Dots. *Phys. Rev. B* **2008**, *77*, 235411.
(57) Fernández-Rossier, J.; Palacios, J. Magnetism in Graphene Nanoislands. *Phys. Rev. Lett.* **2007**, *99*, 177204.

DOI: 10.1021/acs.jpcc.5b03531
J. Phys. Chem. C 2015, 119, 12079−12087

(58) Güçlü, A. D.; Hawrylak, P. Optical Control of Magnetization and Spin Blockade in Graphene Quantum Dots. *Phys. Rev. B* **2013**, *87*, 035425.
(59) Voznyy, O.; Güçlü, A. D.; Potasz, P.; Hawrylak, P. Effect of Edge Reconstruction and Passivation on Zero-Energy States and Magnetism in Triangular Graphene Quantum Dots with Zigzag Edges. *Phys. Rev. B* **2011**, *83*, 165417.
(60) Kurtz, H. A.; Stewart, J. J. P.; Dieter, K. M. Calculation of the Nonlinear Optical Properties of Molecules. *J. Comput. Chem.* **1990**, *11*, 82−87.

DOI: 10.1021/acs.jpcc.5b03531
J. Phys. Chem. C 2015, 119, 12079−12087